

Article

# CFD-Based Comparison Study of a New Flow Diverting Stent and Commercially-Available Ones for the Treatment of Cerebral Aneurysms

Borja Catalán-Echeverría <sup>1</sup>, Michael E. Kelly <sup>2</sup>, Lissa Peeling <sup>2</sup>, Donald Bergstrom <sup>3</sup>,  
Xiongbiao Chen <sup>3,4</sup> and Mauro Malve <sup>1,5,6,\*</sup> 

<sup>1</sup> Department of Engineering, Campus Arrosadía s/n, Public University of Navarra, E-31006 Pamplona, Spain; borja.catalan.echeverria@gmail.com

<sup>2</sup> Department of Surgery, College of Medicine, Royal University Hospital, University of Saskatchewan, 107 Wiggins Road, Suite B419 Health Science Building, Saskatoon, SK S7N 5E5, Canada; m.kelly@usask.ca (M.E.K.); lissa.peeling@usask.ca (L.P.)

<sup>3</sup> Department of Mechanical Engineering, College of Engineering, University of Saskatchewan, Engineering Building 57, Campus Drive, Saskatoon, SK S7N 5A9, Canada; don.bergstrom@usask.ca (D.B.); xbc719@mail.usask.ca (X.C.)

<sup>4</sup> Division of Biomedical Engineering, College of Engineering, University of Saskatchewan, Engineering Building 57, Campus Drive, Saskatoon, SK S7N 5A9, Canada

<sup>5</sup> CIBER-BBN, Research Networking in Bioengineering, Biomaterials & Nanomedicine, C/Mariano Esquillor s/n, E-50018 Zaragoza, Spain

<sup>6</sup> Aragón Institute of Engineering Research (i3A), Universidad de Zaragoza, C/María de Luna s/n, E-50018 Zaragoza, Spain

\* Correspondence: mauro.malve@unavarra.es

Received: 14 February 2019; Accepted: 25 March 2019; Published: 30 March 2019



**Abstract:** Flow-diverting stents (FDSs) show considerable promise for the treatment of cerebral aneurysms by diverting blood flow away from the aneurysmal sacs, however, post-treatment complications such as failure of occlusion and subarachnoid haemorrhaging remain and vary with the FDS used. Based on computational fluid dynamics (CFD), this study aimed to investigate the performance of a new biodegradable stent as compared to two metallic commercially available FDSs. CFD models were developed for an idealized cerebral artery with a sidewall aneurysmal sac treated by deploying the aforementioned stents of different porosities (90, 80, and 70%) respectively. By using these models, the simulation and analysis were performed, with a focus on comparing the local hemodynamics or the blood flow in the stented arteries as compared to the one without the stent deployment. For the comparison, we computed and compared the flow velocity, wall shear stress (WSS) and pressure distributions, as well as the WSS related indices, all of which are of important parameters for studying the occlusion and potential rupture of the aneurysm. Our results illustrate that the WSS decreases within the aneurysmal sac on the treated arteries, which is more significant for the stents with lower porosity or finer mesh. Our results also show that the maximum WSS near the aneurysmal neck increases regardless of the stents used. In addition, the WSS related indices including the time-average WSS, oscillatory shear index and relative residence time show different distributions, depending on the FDSs. Together, we found that the finer mesh stents provide more flow reduction and smaller region characterized by high oscillatory shear index, while the new stent has a higher relative residence time.

**Keywords:** cerebral aneurysm; CFD; flow diverting stent; mass flow reduction; hemodynamics

## 1. Introduction

A cerebral aneurysm, also known as a brain aneurysm, is an abnormal blood-filled bulge or dome of a blood vessel, typically an artery, caused by weakening of the blood vessel due to cerebrovascular diseases/disorders. If untreated, a cerebral aneurysm presents a high risk of rupture, and may lead to haemorrhagic stroke—a leading cause of disability and death around the world. The mechanisms behind the formation and developing of aneurysms have not been fully understood, but there is evidence that high shear stress and blood velocity may provide the hemodynamic environment for degenerative vascular injury [1]. The implantation of an intravascular device in the damaged vessel has been proposed as a way to prevent the developing of the aneurysm and its possible rupture. Among various devices, the flow-diverting stent (FDS), a self-expandable, strut-braided, mesh device, is presently widely used for treating aneurysms, where intra-aneurysmal flow reduction induces progressive aneurysm thrombosis in most patients. The degree of flow modification necessary to induce a complete aneurysm occlusion among patients is not yet clear due to the complexity involved in the changed hemodynamics upon the use of stents. However, the changed hemodynamics are very important for planning the correct treatment [2–4]. Studies have been recently published regarding this topic and it is generally accepted that the success of FDS treatment with a satisfactory aneurysm occlusion depends on the changed hemodynamics [5,6]. Furthermore, it is recognized the porosity of stents plays an important role in the changed hemodynamics; lower porosity can reduce the blood flow into the aneurysm, thus increasing the likelihood of aneurysm occlusion. On the other hand, lower porosity can increase stent stiffness, thus introducing difficulties in stent deployment as well as the possibility of harming arterial walls from the excessive radial force [7]. Typically, the FDA-approved endovascular stents for cerebral applications have porosities between 80% and 90% [7]. The stent design influences stent performance in reducing the aneurysmal inflow [7,8]. During last decades various evaluations of the hemodynamic changes in an aneurysm due to the presence of FDSs have mostly been conducted in vitro and/or by means of numerical studies. Lieber and coworkers extensively studied the aneurysmal flow circulation in the presence of a FDS, illustrating that the capability of diminishing the inflow is a function of the stent shape and strut diameter [9,10]. Studies on the stent effects on aneurysm circulation have also been carried out by using computational fluid dynamics (CFD) [1,7,8,11–14]. For example, the effects of stent mesh shape were investigated by Aenis et al. [11], Rhee et al. [15] Bando and Berger [16], Stuhne and Steinman [17] and Cebra and Lohner [18]. More recently, Larrabide et al. [19–21] analysed the change of flow pulsatility in the aneurysm post the FDS treatment. Some other studies have investigated and evaluated the flow reduction within aneurysmal sacs, depending on aneurysm morphology [22–24] and inflow rate boundary conditions [25]. Recent studies have investigated the connection between hemodynamics and treatment outcomes [5,26–29]. Although experimental and numerical studies and additional clinical trials have already led to significant advances in this field, the effects on local hemodynamics have not been fully understood [21,26,30]. Besides complete aneurysm occlusions in the majority of the FDS-treatment cases, post surgical and long term aneurysm ruptures have also been reported [31]. In this study we propose a new design of biodegradable coarse-mesh stent and we evaluated its performance, as compared to two finer-mesh commercial stents. The aim of the study is to evaluate its capability of reducing the aneurysmal flow and promoting the desired occlusion. This new stent can be fabricated by the dispensing-based rapid prototyping (DBRP) technique that allows for accurate control over the microstructure of the device, thus facilitating the repeatability and precise control over the stent struts [32,33]. With the aforementioned aim, we have employed CFD to numerically evaluate the flow reduction and hemodynamics variables including the wall shear stress (WSS). In addition to the blood flow velocity and pressure, WSS and WSS-related indices can provide important additional information for assessing aneurysm occlusion, risk of aneurysm rupture, and development of stenosis, which are frequently reported as the complications of FDS treatment [31]. In the present study, we investigated how the fine mesh stent affects the reduction of the WSS related indices including time

average wall shear stress (TAWSS) and oscillatory shear index (OSI) distribution. Also, we suggest the necessity of evaluating flow structures and WSS-related indices for analysing the FDS performance.

## 2. Materials and Methods

### 2.1. Assumptions for Model Development

For the model development in this study, we assume that;

- The blood vessels are rigid and the blood flow is incompressible and of a non-Newtonian fluid.
- The blood simulations are performed as unsteady and laminar.
- The boundary condition, i.e., the time-dependent mass flow is adapted from the literature and imposed at the model inlet and outlet.
- Model extensions have been added to the model for guaranteeing that the blood flow in the region of interest (within the artery) is fully developed.

### 2.2. Geometry: Idealized Aneurysm Model

The vessel considered in this work is an idealized cerebral artery harboring a saccular aneurysm represented in Figure 1. The artery is considered as perfectly straight and a sidewall aneurysmal balloon was added in the middle of the vessel. The arterial dimensions were taken from the literature [7]. The idealized sidewall aneurysm model was created by means of the commercial package Rhinoceros © (Robert McNeel and Associates, Seattle, WA, USA). The model consisted of a spherical sac attached to the side of a straight vessel tube as shown in Figure 1. In particular, the aneurysm diameter was 19 mm while the artery diameter was 4.75 mm. The width of the aneurysm neck was 10.7 mm and the aspect ratio (the maximum height of the dome divided by the width of the aneurysm orifice) was 1.68 [7]. The aneurysm and stent geometries were separately reconstructed by means of the aforementioned software package. Then, these were merged in single geometrical models that were later imported and meshed in Ansys ICEM-CFD, Version 16.0 (ANSYS Inc., Canonsburg, PA, USA) as described in the next section.

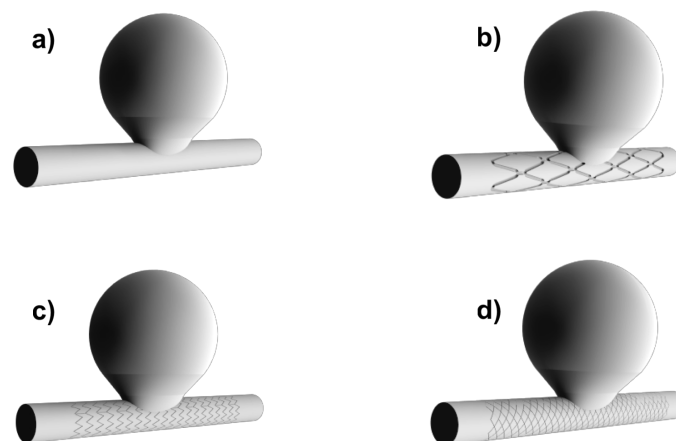


**Figure 1.** Idealized models of the aneurysmal cerebral artery: (a) control case, (b) STENT BS, (c) STENT 1, (d) STENT 2. The aneurysm and artery diameters are 19 mm and 4.75 mm, respectively. The width of the aneurysm neck is 10.7 mm and the aspect ratio (i.e., the maximum height of the dome over the aneurysm width) is 1.68.

### 2.3. Flow Diverting Stents

The new stent and two higher-porosity commercial stents were considered in this study. The commercial devices are representatives of commercially-available stents with T- and W-screen, respectively. The W-screen stent (STENT 1) is manufactured by laser-cutting of a thin-wall tube resulting in rectangular strut cross-sections, while the T-screen (STENT 2) is manufactured by

double-helical woven wires with round strut cross-sections. Figure 2 depicts the three devices, where the resulting mesh patterns of the T-screen and W-screen models are shown. The commercial computer aided design (CAD) software Rhinoceros was used to reproduce the three-dimensional geometry of the stents (see Figure 2). The porosities of the stent models are different, around 90% for the new designed device, 80% for the STENT 1 and around 70% for the STENT 2 (see the mesh patterns in Figure 2). The stent porosity was calculated by the ratio of the void surface to the total surface of the stent cylinder [7]. The three stents were of the same length and of the same external vessel diameter for facilitating the cerebral artery merging process. The main dimensions of the three devices are summarized in Table 1. The new device (STENT BS) is a biodegradable polymeric stent with a zig-zag configuration, manufactured with a strand diameter down to 0.4 mm and fabricated by means of the DBRP technique, allowing for a more accurate control over the stent struts yet facilitating its fabrication and repeatability [32]. The conventional methods of fabricating biodegradable stents in fact are typically to braid monofilaments of biodegradable polymer into a tubular structure [34], which are time-consuming, expensive, and lacking precise control over the device microstructure [35,36]. Notably, the aforementioned new stent is of a design that is inspired by conventional commercial devices but it is particularly suitable to be fabricated from biodegradable materials by means of the DBRP technique [32].

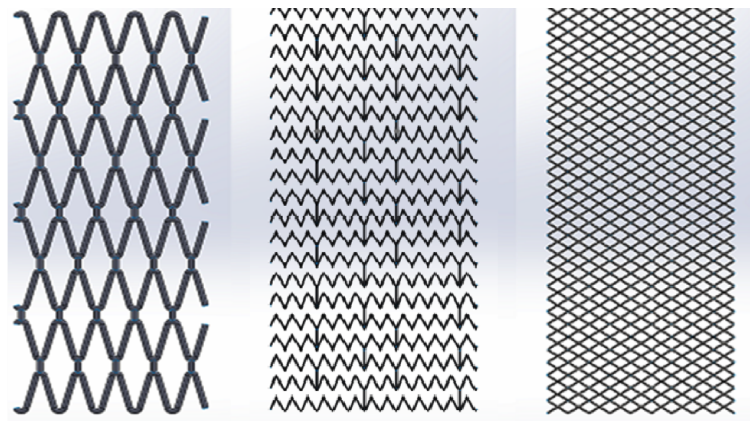


**Figure 2.** Mesh patterns of the considered FDSs with different porosities (90, 80, and 70%). From the left to the right are STENT BS, STENT 1 and STENT 2.

**Table 1.** Dimensions of the flow diverting stents used.

	Thickness (mm)	Length (mm)	Diameter (mm)
STENT BS	0.4	40	4.75
STENT 1	0.1	40	4.75
STENT 2	0.1	40	4.75

#### 2.4. Numerical Analysis

The computational meshes were generated using the commercial software Ansys ICEM CFD, Version 16.0 (ANSYS Inc., Canonsburg, PA, USA). Due to the complexity of the geometry in the presence of stents, the grids were composed of unstructured tetrahedral elements. Finer mesh with smaller tetrahedral elements were used to resolve the stent struts (see Figure 3). To ensure independent results from the mesh element size, a mesh independency study was carried out by using the mesh convergence criterion based on the WSS and the intra-aneurysmal velocity. In particular, we considered it as converged if the mesh results in WSS and velocity profiles within 2.5% from the finest tested mesh [21]. Convergence was reached with an element size around the stent strut of 0.015 mm and a global tetrahedral element size of 0.3 mm. The total number of mesh elements ranged from  $0.4 \times 10^6$  to  $12 \times 10^6$  elements for both untreated and treated models. Unsteady CFD simulations for both

treated and untreated geometrical models were carried out on the commercial software Ansys CFX, Version 16.0 (Ansys Inc., Canonsburg, PA, USA). Notably, in many previous studies of computational hemodynamics of cerebral aneurysm, the blood is simplified of being a Newtonian fluid, which may not be always true [11,37]. For improvement, in the present study we took the rheology of a non-Newtonian fluid into account by employing the constitutive model in which the dynamic viscosity decreases as the shear rate increases. In particular, we used the Carreau-Yasuda model that has been demonstrated as more appropriate than the Newtonian model for low shear rates [37,38]. The constitutive equation of the Carreau-Yasuda model is given by [39–41]:

$$\mu = \mu_{\infty} + (\mu_0 - \mu_{\infty}) \left[ 1 + (\lambda \dot{\gamma})^a \right]^{\frac{n-1}{a}} \quad (1)$$

where  $\mu_0 = 0.056$  is the viscosity at zero shear rate expressed in  $[Pa \cdot s]$ ,  $\mu_{\infty} = 0.00345$  is the viscosity for an infinite shear rate expressed in  $[Pa \cdot s]$ ,  $\lambda = 3.313$  is the relaxation time expressed in  $[s]$ ,  $n = 2$  is the power exponent and  $a = 0.64$  is the Yasuda exponent [39]. The blood density was set to  $1050 \text{ kg/m}^3$ . The vessel wall was assumed to be rigid with a no-slip boundary condition. A flow rate waveform was used as the inlet and outlet conditions, since the model is not compliant. In particular, a time-dependent velocity waveform in an intracranial aneurysmatic cerebral artery was taken from literature [42]. This waveform was adapted to our models for computing the mass flow at the inlet. The obtained waveform that represents a time-dependent mass flow was imposed at the inlet and at the outlet of the model, which were extended to ensure fully developed flow in the region near the stent and the aneurysm. The resultant time dependent mass flow is represented in Figure 3a). Cardiac cycles of 1 s were discretized in time steps of 0.001 s. The main variables such as velocity and pressure were set initially to zero for facilitating convergence. To reduce the effect of initial transients at the beginning of the computation, three complete cardiac cycles were computed and data from the last one was stored for subsequent analysis [19,21]. Typically, the results could be influenced by the convergence obtained at the beginning of the simulations and by the initialization of the variables (either automatic or user-defined). Computing three consecutive cardiac cycles assures a convergent solution and transient-independent results.

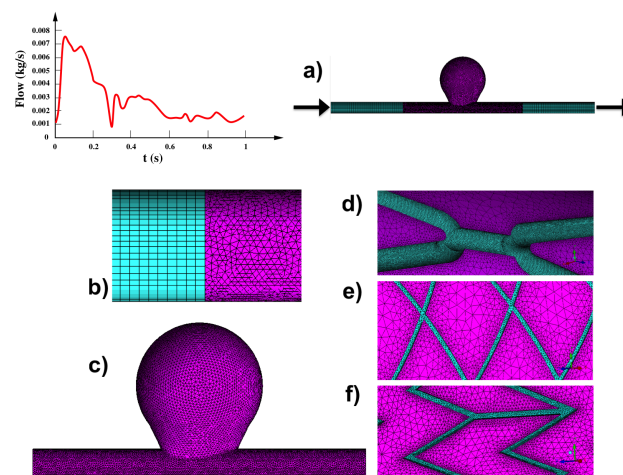


**Figure 3.** Model computational domains. (a) control case (in purple) including extensions (in light blue) and time-dependent mass flow extracted by [42] imposed at the inlet and at the outlet of the models. (b) Close-up view on the interface between the tetrahedral elements of the artery (in purple) and the hexahedral elements of the extension (in light blue). (c) Close-up view on the aneurysm and on the region of interest of the artery (in purple). (d–f) Close-up views showing local refinement around the stent struts for the three flow diverters.

### 2.5. Hemodynamics Parameters

The WSS and its related indices has been extensively used in human hemodynamics for studying the performance of coronary stents [40,41,43–49]. Although they have been used as significant morphologic and hemodynamic parameters for assessing intracranial aneurysm rupture [50–52], their application for evaluating the performance of FDSs has been rarely performed. In general, the blood flow field and pressure have been used as parameters to assess the performance of the FDS treatment [1,3,4,8,20–22,53]. In this regard, we believe that it is rational to evaluate WSS-related variables to quantify the changed hemodynamics upon the stent implantation. By using the aforementioned models, we evaluated velocity, pressure and WSS-related variables such as time average wall shear stress (TAWSS), oscillatory shear index (OSI) and relative residence time (RRT). As noted previously, all the variables were evaluated during the third computed cardiac cycle for each aneurysm with or without the deployment of a FDS. All hemodynamic factors were registered at every time step. The WSS-related variables were computed starting from the instantaneous WSS vector  $\vec{\tau}_w$  registered at each time instant of the cardiac cycle ( $T$ ). The TAWSS for a pulsatile flow represents the spatial distribution of the tangential, frictional stress caused by the action of blood flow on the vessel wall temporally averaged on the entire cardiac cycle. It can be calculated by integrating the WSS vector over the cardiac cycle, i.e.,

$$TAWSS = \frac{1}{T} \int_0^T |\vec{\tau}_w| dt \quad (2)$$

The OSI is a non-dimensional parameter that measures the directional change of WSS during the cardiac cycle [54]. OSI is often used to describe the disturbance of a flow field. It is defined by:

$$OSI = 0.5 \left( 1 - \frac{|\int_0^T \vec{\tau}_w dt|}{\int_0^T |\vec{\tau}_w| dt} \right) \quad (3)$$

A combination of TAWSS and OSI reflects the residence time of blood near the wall as proposed by Himburg et al. [55]. Thus, a new metric termed RRT can be defined to quantify the state of disturbed flow:

$$RRT = \frac{1}{(1 - 2 \cdot OSI) \cdot TAWSS} = \frac{1}{\frac{1}{T} |\int_0^T \vec{\tau}_w dt|} \quad (4)$$

RRT is an additional hemodynamic factor to describe the slow fluid motion near the aneurysm wall [54,56]. It is especially important when considering vascular diseases such as aneurysms because the reduction of blood flow within the aneurysm sac is the principal role played by FDSs. As such, this index can provide the measurement of the flow blockage that leads to the thrombosis post the stent treatment.

### 3. Results

In the present study, the mean velocity of blood flow within the sac as well as the wall shear stress and their associated hemodynamics variables have been computed in order to quantify the influence of different stents. As noted previously, a variety of criteria have been formulated and used in the literature to quantify hemodynamic effects so as to predict the risk of aneurysm rupture. Not only the instantaneous wall shear stress distribution but also its spatial or temporal variation has been considered as the suitable index to predict rupture [50–52]. There is no real agreement within the research community about the most relevant parameters yet [22]. In this work, classical hydrodynamic quantities were computed and combined to represent the changed hemodynamics in the cerebral aneurysm after the FDS treatment. In particular, the residual residence time RRT was evaluated and used to quantify the tendency toward thrombus formation [7], thus allowing the evaluation of the FDSs performance. The flow structures and the spatial distribution of the pressure and of the WSS-related indices are depicted in Figures 4–6. The main values quantified from Figure 7 are listed in the Table 2.

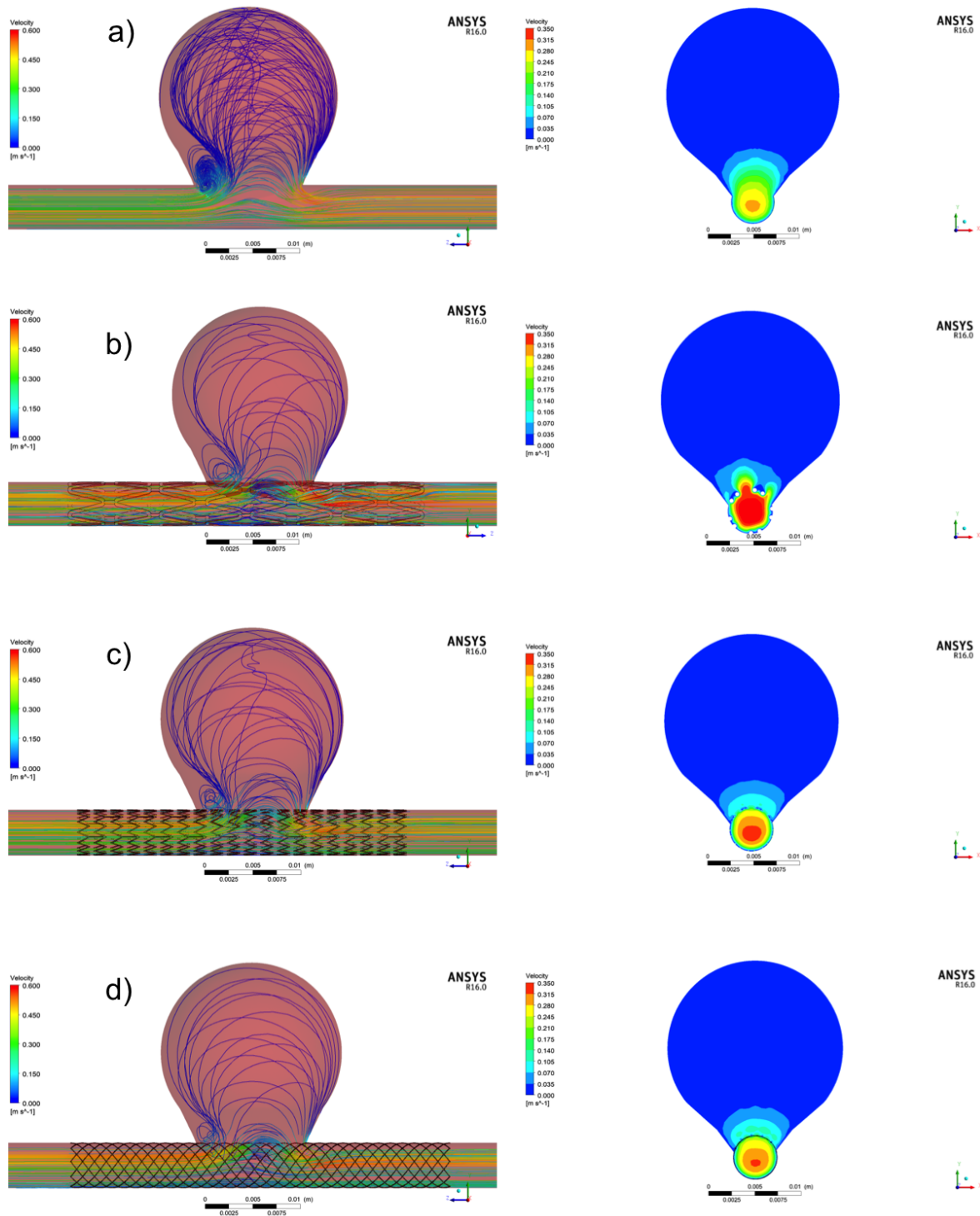


**Figure 4.** On the left are the streamlines emitted from inlet and neck colored with the local velocity magnitude, on the right are the velocity magnitude depicted on a transverse plane; for the cases of (a) control case, (b) STENT BS, (c) STENT 1, and (d) STENT 2.

**Table 2.** Summary of the simulation results.

	Flow (Kg/s) (mm)	Max TAWSS (mm)	Max OSI (mm)	Max RRT (mm)
<b>Control case</b>	$1.28 \times 10^{-6}$	3.43	0.49	41.09
<b>STENT BS</b>	$6.75 \times 10^{-8}$	5.09	0.48	54.25
<b>STENT 1</b>	$4.47 \times 10^{-8}$	4.29	0.48	48.42
<b>STENT 2</b>	$3.82 \times 10^{-8}$	3.56	0.47	42.42

3.1. Aneurysm without Treatment: Control Case

In Figure 4 the streamlines colored with the local velocity magnitude are shown in the aneurysmatic sac before treatment. Coinciding with other studies [22,57], the blood flow within the aneurysm enters from the distal portion of the aneurysm neck and swirls around the periphery of the aneurysm sac with a slower velocity. Finally, the flow leaves the sac in the proximal region around the inflow zone (see Figure 4a). The pressure within the sac is almost constant and similar between the control case and the stented cases (see Figure 5). Also, in agreement with the previous study [24], the pressure drop is very small despite the presence of the aneurysm. The WSS at the peak flow of the cardiac cycle is almost constant along the parent vessel upstream of the aneurysm except at the entrance of the sac, where the changes in velocity direction are registered. In the sac, much smaller WSS values were found in comparison with the vessel, as reflected by the TAWSS (see Figure 6a). As an average computed variable, the TAWSS attenuates and smooths the spatial differences. Larger values are depicted at the junction of the artery with the neck. The maximum TAWSS is found at the bottom of the proximal neck region, with a maximum value around 6 Pa, almost two times of the value observed in the parent vessel just upstream of the aneurysm. The OSI for the untreated artery had large values in the proximal region of the sac near to the vessel. This finding agrees with previous studies, indicating that high OSI is of an aneurysmal risk factor [50]. Finally the RRT shows higher values and hence higher residence of flow particles at the top of the sac. From the theoretical point of view, it is believed that for an aneurysmal flow with vortical structures, the flow near the wall tends to be recirculating, slow, and oscillatory. Thus, the average TAWSS tends to be low while the OSI tends to be high. The area exposed to low shear stress tends to be large and the time spent by the fluid particles near the wall tends to increase provoking a high RRT.

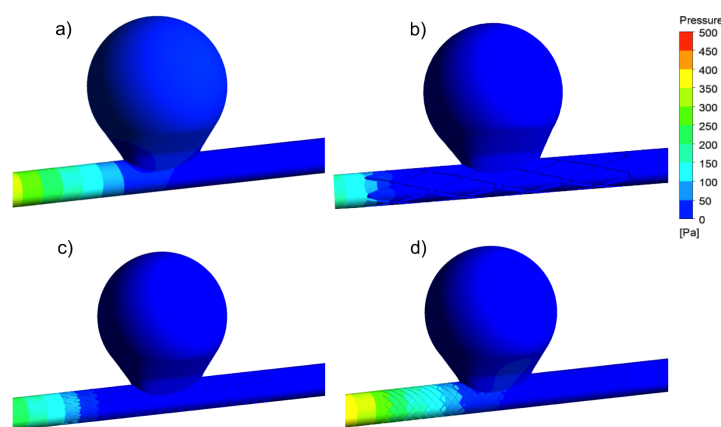


**Figure 5.** Pressure contours for the cases of (a) control case, (b) STENT BS, (c) STENT 1, and (d) STENT 2.

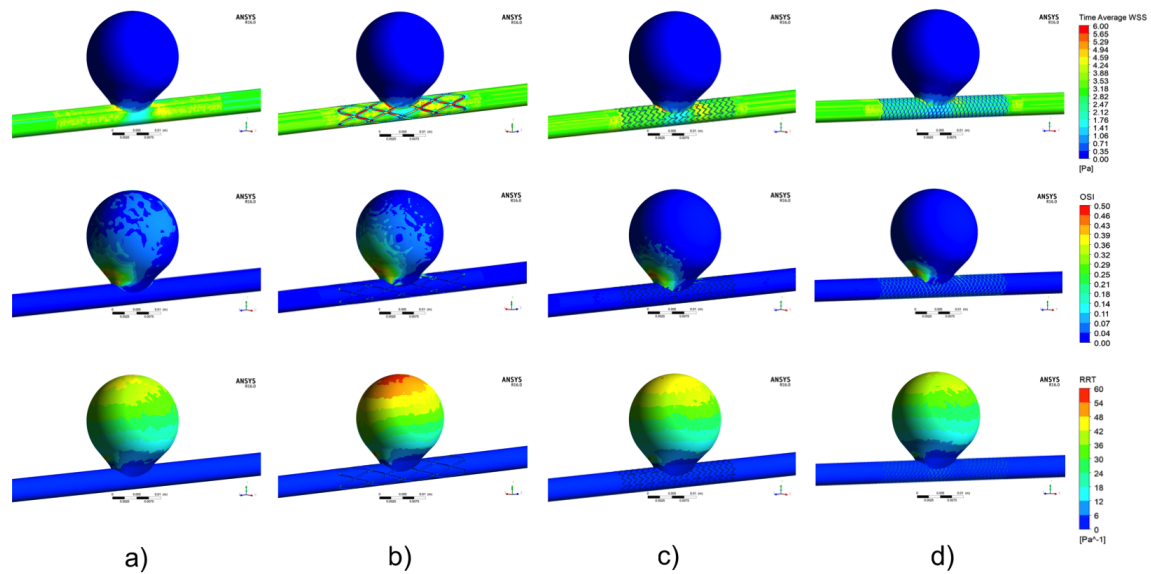


**Figure 6.** First row are the spatial distribution of the TAWSS, second row are the spatial distribution of the OSI, and third row are the spatial distribution of the RRT; for the cases of (a) control case, (b) STENT BS, (c) STENT 1, and (d) STENT 2.

### 3.2. Aneurysm under FDS Treatment: Flow and Velocity Field

Stenting leads to considerable hemodynamic modifications as shown by the reduction of peak velocities (compare Figure 4a to Figure 4b–d). The reverse flow (from left to right) near the aneurysm dome becomes slowdown, which is more profound with the case of STENT 2. Before leaving the sac in a direction almost parallel to the upper wall of the parent vessel, the flow accelerates slightly. The observed streamlines at the peak flow during the cardiac cycle within the sac are of indications of a high stenting efficiency, particularly for the case of STENT 2. The reduction of peak velocity and of the flow inside the sac provokes an increase of the flow inside the vessel as visible in Figure 4a–d through 3D velocity streamlines and 2D velocity magnitudes depicted on transversal planes. This increase is particularly significant for the new designed biodegradable stent. However, the new design has a higher porosity and as such, affects the flow reduction as compared to the other two stents (Figure 4b and Figure 4c,d). It is noted that the degree of reduction and the distribution of flow through the neck depend on the orientation of stent struts [58,59]. The reduction of mass flow inside the aneurysmatic sac is shown in Figure 7a for the cases of stents as compared to the untreated aneurysms. It is seen that a significant reduction of flow is achieved with all stents, especially for case of STENT 2.

### 3.3. Aneurysm under FDS Treatment: TAWSS Distribution

The results show a slight reduction of TAWSS within the aneurysm sac for all stented cases. However, around the neck of the sac a general increase of very small regions of high TAWSS is seen for all stented arteries (Figure 7b). Generally, the results presented in the first row of Figure 6a show the trends similar to those already discussed concerning the mean velocity (Figure 4a). In all cases, stenting leads to the reduction of peak WSS and, as a consequence, of the TAWSS within the aneurysm sac (Figure 6a–d). This reduction, however, is not much different among the three stents seem, indicating their similar performance in this regard. The increase at the aneurysmal neck for all stented cases may have lead to the possible rupture of the aneurysm after treatment. These regions seem less accentuated for the case of STENT 2.

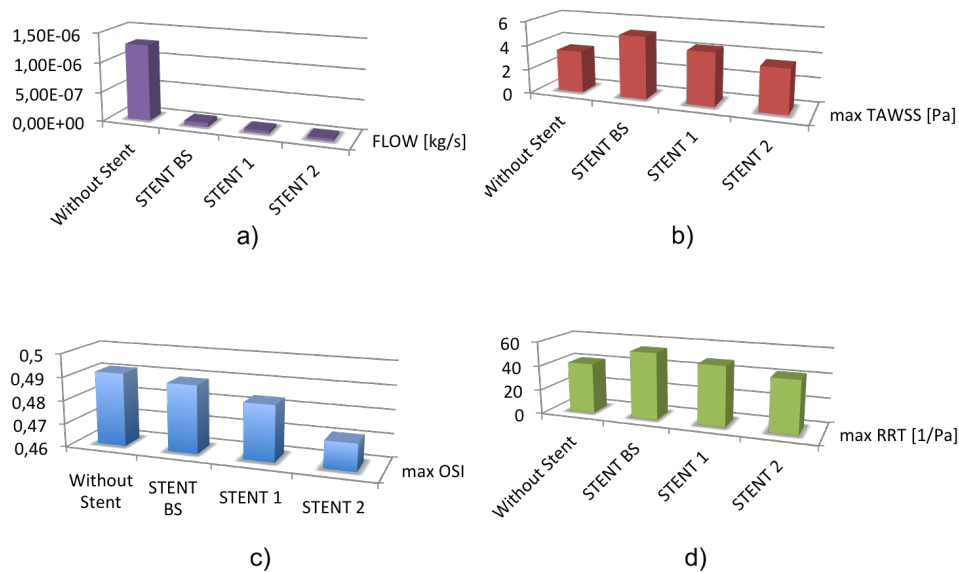


**Figure 7.** (a) Flow reduction promoted by FDSs, (b) peak TAWSS, (c) OSI, and (d) RRT (d) in the aneurysmatic sac for the artery without treatment and in the presence of the three considered stents.

### 3.4. Aneurysm under FDS Treatment: OSI Distribution

In the literature it was reported that the value of OSI for ruptured aneurysm is higher than that for unruptured aneurysms [50]. For evaluating the performance of FDS, OSI is of a meaningful parameter to be taken into account. In this work, we evaluated the OSI for each treated aneurysm, as compared to the case without treatment (Figure 6). We noticed the region of high OSI proximal to the sac, which may be caused by the recirculation inside the aneurysm. The variation of peak OSI is shown in Figure 7c. It is seen that all stents promote a slight reduction of this variable and that the case of STENT 2 has the best result. From Figure 6 we can also see that all stents are capable of reducing the highest OSI region and that this reduction is accentuated for the case of STENT 2 and more attenuated for the other two cases (i.e., STENT BS and STENT 1).

### 3.5. Aneurysm under FDS Treatment: RRT Distribution

From the stenting-efficiency point of view, the RRT is of the most interesting variable as it is a measurement of the relative increase of blood residence time within the aneurysm sac. This variable allows for the global analysis of hemodynamic changes and thrombus formation in the sac [22]. In the Figure 6 it can be seen that stenting leads to an increase of RRT within the aneurysm sac. STENT 2 with a low porosity shows a similar spatial distribution with respect to the control case; while STENT 1 has higher values. The biodegradable stent seems to provide the largest increase in RRT (by comparing the third row of Figure 6d with Figure 6a to Figure 6c). This increase may be explained by the large high OSI region caused by the biodegradable stent due to the lower diverted flow and the induced change in flow structures (Figure 4a–d). As reported by Himburg et al. [55], high RRT is characterized by low velocity with low WSS and oscillatory flow with high OSI. OSI is insensitive to WSS magnitude; locations with low WSS could not necessarily be identified as sites of high OSI because low WSS may simply results from a decrease of the flow velocity without any local flow recirculation. Our results shows that the high RRT in the case of biodegradable stent is reached with low, but not oscillatory, WSS and high OSI around the aneurysmal dome. From the third row of Figure 6, it is seen that the highest RRT values are reached in very small locations near to the aneurysmal neck. This is due to the local oscillation of the flow, as seen from the streamlines (Figure 4). As a result, at the same location, all stented arteries have higher OSI values than the one without stent. The variation of peak RRT for the different stents is shown in Figure 7d. It is seen that PRT reached

its maximal value at the dome rather than the area near the neck and among them, STENT 2 has the highest RRT. These results suggest the necessity of computing the RRT so as to provide the information on the flow motion near the aneurysmatic wall as well as the information on the FDS-induced flow blockage inside the aneurysmatic sac as reflected by OSI.

#### 4. Discussion

In the recent years, the endovascular techniques for treating cerebral aneurysms have shown significant advances although, they still need to be improved [22]. Intravascular stenting is presently one of the most used treatment methods even though their effect on the flow has not been completely explained from the scientific point of view. For treating cerebral aneurysms with flow diverters, a deep knowledge of the associated hemodynamic changes is always needed for optimizing the treatment performance of the stents. FDSs are considered promising for reducing blood flow into and thus occluding the aneurysmatic sac. While in the past these devices were used in association with other techniques, many studies have demonstrated that they can be potentially used alone [8,10,11,58]. Also, it has been shown that the porosity has emerged as one of the very important parameters for the success of FDS treatment [1,7,9]. This parameter is important to the hemodynamics changes in the artery, such as the changes in blood flow velocity and pressure, thus affecting the thrombosis. Despite many encouraging studies, the outcomes of cerebral aneurysms treated by FDSs remain uncertain and unpredictable. For example, some modifications that could be induced by the FDS for facilitating the desired hemodynamic environment are still unknown [4,22,50]. Very recently Ouared et al. [4] investigated the aneurysmal hemodynamic changes before and after FDS treatment; and they also examined the potential hemodynamic reduction thresholds by analysing velocity, WSS, and pressure pre- and post- stent treatments. Furthermore, they suggested a velocity reduction threshold for the aneurysm thrombosis. Unfortunately, no other hemodynamic indices have been reported in this regard. Only a few studies have analyzed the WSS related variables [50,52] and used them in assessing aneurysmal rupture [22,29]. A better understanding of the post treatment conditions would help the design of new devices for treating aneurysms. For this, in this work we have analyzed various hemodynamics quantities (velocity, pressure, TAWSS, OSI and RRT) within an idealized cerebral aneurysmatic artery in the presence of a new FDS design. Its performance has been compared with those of other commercial designs. The hemodynamic variables examined in this study could help identify the risk of aneurysm rupture [50]. In particular, TAWSS and OSI are recognized to be strong indicators for determining whether or not an aneurysm will rupture as reported by Xiang et al. [50]. Previous studies have demonstrated that low WSS and high OSI regulate endothelial surface adhesion molecules, causing dysfunction of flow-induced nitrous oxide, increasing endothelial permeability, and thus, promoting atherogenesis and inflammatory cell infiltration [60]. The inflammation process caused by this hemodynamic environment may promote degradation of the aneurysm wall, and possibly lead to the aneurysm rupture [50,60]. In this study we also compute the RRT, which is associated with the flow blockage in the aneurysm. This parameter is directly correlated with TAWSS and OSI and has been very rarely evaluated for assessing FDS performance though it can provide the information on of the flow motion near the arterial wall. The biodegradable stent showed the largest increase in RRT despite a similar flow reduction due to its larger porosity. This would be explained by examining the OSI spatial distribution on the aneurysmal dome. The maximal value was found in a specific region in all stented cases, the case of STENT BS showed higher values around the dome as compared to the other two cases (STENT 1 and 2). This result suggests the necessity of evaluating the variable of RRT in addition to the flow reduction. Many of previous studies have focused on the blood flow, velocity and pressure. However, WSS-related indices, especially OSI and RRT, are important for assessing the hemodynamics conditions, as modified by the use of FDSs [22], and are able to provide information related to the post-treatment ruptures and/or branch stenosis among other complications [31].

## 5. Limitations

The present study is preliminary and the obtained results are subject to following limitations. Firstly, the reported capability of the stents for reducing the blood flow is based on numerical simulations, which may be premature due to the lack of experimental validation. Even though, our work has successfully developed CFD-based methods for comparing the treatment outcomes of aneurysms treated by different FDSs, with the first insight into the main properties of the considered stents. Secondly, the models and simulation results did not consider the interaction between blood flow and arterial walls, or the arterial compliance and stent geometrical changes. Thus, this study reveals the information on the flow patterns and the WSS indices, rather than the information related to the change of aneurysm structure. Also, the rigid walls could inherently influence flow patterns. However, the importance of the FSI when modelling cerebral aneurysms is still being debated in the literature since the human intracranial arteries are stiffer than other arteries. For this reason, the impact of the vascular motion on the hemodynamics may be limited [42,61]. At last, the idealized virtual stent configurations used in the present work may be different from the real one due to the patient specific artery and other patient conditions.

## 6. Conclusions

In this study, we presented a simplified CFD model consisting of a spherical aneurysm on a straight artery, where three different stents - a new design and two commercial devices, were deployed, respectively, for treatment. Our CFD-based simulation illustrated that the deployment of the stents resulted in the reduction of flow, as indicated by the decrease in the mean velocity within the aneurysm. Our results of WSS-related indices also showed that the finer mesh stent with the lowest porosity had the best performance in terms of the reduced flow, TAWSS and OSI and that the new stent of a more porous construct had a higher RRT, thus likely contributing to the aneurysm occlusion, suggesting its flow structure may be more appropriate. This result also suggests the necessity of evaluating flow structures and WSS-related indices in addition to the capacity of the device of reducing the flow, the WSS and the pressure. It should be noted that, although the aneurysmal model developed in this study is simple, it would serve as a base to develop patient-oriented models for continuing research in this direction.

**Author Contributions:** Study design, X.C., D.B., M.M., L.P. and M.E.K; numerical simulations, B.C.E. and M.M.; data curation, L.P. and M.E.K.; writing—original draft preparation, M.M., X.C. and D.B.; writing—review and editing, M.M., M.E.K., X.C. and D.B.; supervision, X.C. and M.M.

**Funding:** This research was funded by the Saskatchewan Health Research Foundation (SHRF Grant Reference #2784). M. Malvè was supported by the Spanish Ministry of Education, Culture and Sport through the grant PRX17/00335 financed within the National Program ‘Salvador de Madariaga’. The authors also acknowledge the support of the Spanish Ministry of Industry and Competitiveness via the research project DP12017-83259-R (AEI/FEDER, UE) and the Instituto de Salud Carlos III (ISCIII) through the CIBER-BBN initiative.

**Conflicts of Interest:** None of the authors of this work has conflict of interest with other people and organizations. The funders had no role in the design of the study; in the collection, analyses, or interpretation of data; in the writing of the manuscript, or in the decision to publish the results.

## References

1. Kim, Y.H.; Xu, X.; Lee, J.S. The effect of stent porosity and strut shape on saccular aneurysm and its numerical analysis with Lattice Boltzmann method. *Ann. Biomed. Eng.* **2010**, *38*, 2274–2292. [[CrossRef](#)] [[PubMed](#)]
2. Kulcsár, Z.; Augsburger, L.; Reymond, P.; Pereira, V.M.; Hirsch, S.; Mallik, A.S.; Millar, J.; Wetzel, S.G.; Wanke, I.; Rüfenacht, D.A. Flow diversion treatment: Intra-aneurysmal blood flow velocity and WSS reduction are parameters to predict aneurysm thrombosis. *Acta Neurochir. Wien* **2012**, *154*, 1827–1834. [[CrossRef](#)] [[PubMed](#)]

3. Mut, F.; Raschi, M.; Scrivano, E.; Bleise, C.; Chudyk, J.; Ceratto, R.; Lylyk, P.; Cebal, J.R. Association between hemodynamic conditions and occlusion times after flow diversion in cerebral aneurysms. *J. Neurointerv. Surg.* **2015**, *7*, 286–290. [[CrossRef](#)]
4. Ouared, R.; Larrabide, I.; Brina, O.; Bouillot, P.; Erceg, G.; Yilmaz, H.; Lovblad, K.O.; Mendes Pereira, V. Computational fluid dynamics analysis of flow reduction induced by flow-diverting stents in intracranial aneurysms: A patient-unspecific hemodynamics change perspective. *J. Neurointerv. Surg.* **2016**, *8*, 1288–1293. [[CrossRef](#)] [[PubMed](#)]
5. Lylyk, P.; Miranda, C.; Ceratto, R.; Ferrario, A.; Scrivano, E.; Luna, H.R.; Berez, A.L.; Tran, Q.; Nelson, P.K.; Fiorella, D. Curative endovascular reconstruction of cerebral aneurysms with the pipeline embolization device: the Buenos Aires experience. *Neurosurgery* **2009**, *64*, 632–642. [[CrossRef](#)]
6. Becske, T.; Kallmes, D.F.; Saatci, I.; McDougall, C.G.; Szikora, I.; Lanzino, G.; Moran, C.J.; Woo, H.H.; Lopes, D.K.; Berez, A.L.; et al. Pipeline for uncoilable or failed aneurysms: results from a multicenter clinical trial. *Radiology* **2013**, *267*, 858–868. [[CrossRef](#)] [[PubMed](#)]
7. Kim, M.; Taulbee, D.B.; Tremmel, M.; Meng, H. Comparison of two stents in modifying cerebral aneurysm hemodynamics. *Ann. Biomed. Eng.* **2008**, *36*, 726–741. [[CrossRef](#)]
8. Dholakia, R.; Sadasivan, C.; Fiorella, D.J.; Woo, H.H.; Lieber, B.B. Hemodynamics of flow diverters. *J. Biomech. Eng.* **2017**, *139*, 021002. [[CrossRef](#)]
9. Lieber, B.B.; Stancampiano, A.P.; Wakhloo, A.K. Alteration of hemodynamics in aneurism models by stenting: Influence on stent porosity. *Ann. Biomed. Eng.* **1997**, *25*, 460–469. [[CrossRef](#)]
10. Lieber, B.B.; Livescu, V.; Hopkins, L.N.; Wakhloo, A.K. Particle image velocimetry assessment of stent design influence on intra-aneurysmal flow. *Ann. Biomed. Eng.* **2002**, *30*, 768–777. [[CrossRef](#)] [[PubMed](#)]
11. Aenis, M.; Stancampiano, A.P.; Wakhloo, A.K.; Lieber, B.B. Modeling of flow in a straight stented and nonstented side wall aneurysm model. *J. Biomech. Eng.* **1997**, *119*, 206–212. [[CrossRef](#)]
12. Jou, L.D.; Chintalapani, G.; Mawad, M.E. Metal coverage ratio of pipeline embolization device for treatment of unruptured aneurysms: Reality check. *Interv. Neuroradiol.* **2016**, *22*, 42–48. [[CrossRef](#)] [[PubMed](#)]
13. Li, Y.; Zhang, M.; Verrelli, D.I.; Chong, W.; Ohta, M.; Quian, Y. Numerical simulation of aneurysmal haemodynamics with calibrated porous-medium models of flow-diverting stents. *J. Biomech.* **2018**, *80*, 88–94. [[CrossRef](#)]
14. Zhang, Y.; Wang, Y.; Kao, E.; Flórez-Valencia, L.; Courbebaisse, G. Towards optimal flow diverter porosity for the treatment of intracranial aneurysm. *J. Biomech.* **2019**, *82*, 20–27. [[CrossRef](#)] [[PubMed](#)]
15. Rhee, K.; Han, M.H.; Cha, S.H. Changes of flow characteristics by stenting in aneurysm models: Influence of aneurysm geometry and stent porosity. *Ann. Biomed. Eng.* **2002**, *30*, 894–904. [[CrossRef](#)]
16. Bando, K.; Berger, S.A. Research on fluid-dynamic design criterion of stent used for treatment of aneurysms by means of computational simulation. *Comp. Fluid Dyn. J.* **2003**, *11*, 527–531.
17. Stuhne, G.R.; Steinman, D.A. Finite-element modeling of the hemodynamics of stented aneurysms. *J. Biomech. Eng.* **1997**, *126*, 382–387. [[CrossRef](#)]
18. Cebal, J.R.; Lohner, R. Efficient simulation of blood flow past complex endovascular devices using an adaptive embedding technique. *IEEE Trans. Med. Imaging* **2005**, *24*, 468–476. [[CrossRef](#)]
19. Larrabide, I.; Aguilar, M.L.; Morales, H.G.; Geers, A.J.; Kulcsár, Z.; Rüfenacht, D.A.; Frangi, A.F. Intra-aneurysmal pressure and flow changes induced by flow diverters: Relation to aneurysm size and shape. *AJNR Am. J. Neuroradiol.* **2013**, *34*, 816–822. [[CrossRef](#)] [[PubMed](#)]
20. Larrabide, I.; Geers, A.J.; Morales, H.G.; Aguilar, M.L.; Rüfenacht, D.A. Effect of aneurysm and ICA morphology on hemodynamics before and after flow diverter treatment. *J. Neurointerv. Surg.* **2015**, *7*, 272–280. [[CrossRef](#)] [[PubMed](#)]
21. Larrabide, I.; Geers, A.J.; Morales, H.G.; Bijlenga, P.; Rüfenacht, D.A. Change in aneurysmal flow pulsatility after flow diverter treatment. *Comput. Med. Imaging Graph.* **2016**, *50*, 2–8. [[CrossRef](#)]
22. Seshadhri, S.; Janiga, G.; Beuing, O.; Skalej, M.; Thevenin, D. Impact of stents and flow diverters on hemodynamics in idealized aneurysm models. *J. Biomech. Eng.* **2011**, *133*, 071005. [[CrossRef](#)] [[PubMed](#)]
23. Wu, Y.F.; Yang, P.F.; Shen, J.; Huang, Q.H.; Zhang, X.; Qian, Y.; Liu, J.M. A comparison of the hemodynamic effects of flow diverters on wide-necked and narrow-necked cerebral aneurysms. *J. Clin. Neurosci.* **2012**, *19*, 1520–1524. [[CrossRef](#)] [[PubMed](#)]

24. Wang, C.; Tian, Z.; Liu, J.; Jing, L.; Paliwal, N.; Wang, S.; Zhang, Y.; Xiang, J.; Siddiqui, A.H.; Meng, H.; et al. Flow diverter effect of LVIS stent on cerebral aneurysm hemodynamics: A comparison with Enterprise stents and the Pipeline device. *J. Transl. Med.* **2016**, *14*, 199. [[CrossRef](#)] [[PubMed](#)]
25. Mut, F.; Ruijters, D.; Babic, D.; Bleise, C.; Lylyk, P.; Cebral, J.R. Effects of changing physiologic conditions on the in vivo quantification of hemodynamic variables in cerebral aneurysms treated with flow diverting devices. *Int. J. Numer. Method Biomed. Eng.* **2014**, *30*, 135–142. [[CrossRef](#)] [[PubMed](#)]
26. Cebral, J.R.; Mut, F.; Raschi, M.; Scrivano, E.; Ceratto, R.; Lylyk, P.; Putman, C.M. Aneurysm rupture following treatment with flow-diverting stents: Computational hemodynamics analysis of treatment. *AJNR Am. J. Neuroradiol.* **2011**, *32*, 27–33. [[CrossRef](#)]
27. Mut, F.; Cebral, J.R. Effects of flow-diverting device oversizing on hemodynamics alteration in cerebral aneurysms. *AJNR Am. J. Neuroradiol.* **2012**, *33*, 2010–2016. [[CrossRef](#)]
28. Zhang, Y.; Chong, W.; Qian, Y. Investigation of intracranial aneurysm hemodynamics following flow diverter stent treatment. *Med. Eng. Phys.* **2013**, *35*, 608–615. [[CrossRef](#)] [[PubMed](#)]
29. Levitt, M.R.; McGah, P.M.; Aliseda, A.; Mourad, P.D.; Nerva, J.D.; Vaidya, S.S.; Morton, R.P.; Ghodke, B.V.; Kim, L.J. Cerebral aneurysms treated with flow-diverting stents: Computational models with intravascular blood flow measurements. *AJNR Am. J. Neuroradiol.* **2014**, *35*, 143–148. [[CrossRef](#)]
30. Pereira, V.M.; Bonnefous, O.; Ouared, R.; Brina, O.; Stawiaski, J.H.; Aerts, H.; Ruijters, D.; Narata, A.P.; Bijlenga, P.; Schaller, K.; et al. A DSA-based method using contrast-motion estimation for the assessment of the intra-aneurysmal flow changes induced by flow-diverter stents. *AJNR Am. J. Neuroradiol.* **2013**, *34*, 808–815. [[CrossRef](#)]
31. Seibert, B.; Tummala, R.P.; Chow, R.; Faridar, A.; Mousavi, S.A.; Divani A.A. Intracranial aneurysms: Review of current treatment options and outcomes. *Front. Neurol.* **2011**, *2*, 1–11. [[CrossRef](#)]
32. Han, X.; Wu, X.; Kelly, M.; Chen, X.B. Fabrication and optimal design of biodegradable polymeric stents for aneurysms treatments. *J. Funct. Biomater.* **2017**, *8*, 8. [[CrossRef](#)]
33. Chen, X.B. *Extrusion Bioprinting of Scaffolds for Tissue Engineering Applications*; Springer International Publishing AG: Cham, Switzerland, 2019.
34. Waksman, R. Biodegradable stents: They do their job and disappear. *J. Invasive Cardiol.* **2006**, *18*, 70–74. [[PubMed](#)]
35. Chen, X.B.; Li, M.; Ke, H. Modeling of the flow rate in the dispensing-based process for fabricating tissue scaffolds. *J. Manuf. Sci. Eng.* **2008**, *130*, 021003. [[CrossRef](#)]
36. Li, M.G.; Tian, X.Y.; Chen, X.B. A brief review of dispensing-based rapid prototyping techniques in tissue scaffold fabrication: Role of modeling on scaffold properties prediction. *Biofabrication* **2009**, *1*, 032001. [[CrossRef](#)]
37. Johnston, B.M.; Johnston, P.R.; Corney, S.; Kilpatrick, D. Non-Newtonian blood flow in human right coronary arteries: Steady state simulations. *J. Biomech.* **2004**, *37*, 709–720. [[CrossRef](#)]
38. Johnston, B.M.; Johnston, P.R.; Corney, S.; Kilpatrick, D. Non-Newtonian blood flow in human right coronary arteries: Transient simulations. *J. Biomech.* **2006**, *39*, 1116–1128. [[CrossRef](#)]
39. Valencia, A.; Villanueva, M. Unsteady flow and mass transfer in models of stenotic arteries considering fluid-structure interaction. *Int. Commun. Heat Mass Transf.* **2006**, *33*, 966–975. [[CrossRef](#)]
40. Morlacchi, S.; Chiastra, C.; Gastaldi, D.; Pennati, G.; Dubini, G.; Migliavacca, F. Sequential structural and fluid dynamic numerical simulations of a stented bifurcated coronary artery. *J. Biomech. Eng.* **2011**, *133*, 121010. [[CrossRef](#)]
41. Chiastra, C.; Morlacchi, S.; Gallo, D.; Morbiducci, U.; Cárdenes, R.; Larrabide, I.; Migliavacca, F. Computational fluid dynamic simulations of image-based stented coronary bifurcation models. *J. R. Soc. Interfaces* **2013**, *10*, 20130193. [[CrossRef](#)] [[PubMed](#)]
42. Torii, R.; Oshima, M.; Kobayashi, T.; Takagi, K.; Tezduyar, T.E. Fluid-structure interaction modeling of blood flow and cerebral aneurysm: Significance of artery and aneurysm shapes. *Comp. Meth. Appl. Mech. Eng.* **2009**, *198*, 3613–3621. [[CrossRef](#)]
43. LaDisa, J.; Guler, I.; Olson, L. 3D computational fluid dynamics modeling of alterations in coronary wall shear stress produced by stent implantation. *Ann. Biomed. Eng.* **2003**, *31*, 972–980. [[CrossRef](#)]
44. LaDisa, J.; Hettrick, D.; Olson, L. Stent implantation alters coronary artery hemodynamics and wall shear stress during maximal vasodilation. *J. Appl. Physiol.* **2002**, *93*, 1939–1946. [[CrossRef](#)]

45. LaDisa, J.; Hettrick, D.; Olson, L.; Hettrick, D.; Warltier, D.; Kersten, J.; Pagel, P. Alterations in regional vascular geometry produced by theoretical stent implantation influence distributions of wall shear stress: Analysis of a curved coronary artery using 3D computational fluid dynamics modeling. *Biomed. Eng. Online* **2006**, *5*, 40. [[CrossRef](#)]
46. Masson, I.; Boutouyrie, P.; Laurent, S.; Humphrey, J.; Zidi, M. Characterization of arterial wall mechanical behavior and stresses from human clinical. *J. Biomech.* **2008**, *41*, 2618–2627. [[CrossRef](#)]
47. Brindise, M.; Chiastra, C.; Burzotta, F.; Migliavacca, F.; Vlachos, P. Hemodynamics of stent implantation procedures in coronary bifurcations: An In Vitro study. *Ann. Biomed. Eng.* **2017**, *45*, 542–553. [[CrossRef](#)]
48. Simão, M.; Ferreira, J.M.; Mora-Rodríguez, J.; Fragata, J.; Ramos, H.M. Behaviour of two typical stents towards a new stent evolution. *Med. Biol. Eng. Comp.* **2017**, *55*, 1019–1037. [[CrossRef](#)]
49. Simão, M.; Ferreira, J.M.; Mora-Rodríguez, R.H.M. Structural analysis of two different stent configurations. *Comp. Meth. Biomech. Biomed. Eng.* **2017**, *20*, 869–883. [[CrossRef](#)]
50. Xiang, J.; Natarajan, S.K.; Tremmel, M.; Ma, D.; Mocco, J.; Hopkins, L.N.; Siddiqui, A.H.; Levy, E.I.; Meng, H. Hemodynamic-morphologic discriminants for intracranial aneurysm rupture. *Stroke* **2011**, *42*, 144–152. [[CrossRef](#)]
51. Kawaguchi, T.; Nishimura, S.; Kanamori, M.; Takazawa, H.; Omodaka, S.; Sato, K.; Maeda, N.; Yokoyama, Y.; Midorikawa, H.; Sasaki, T.; et al. Distinctive flow pattern of wall shear stress and oscillatory shear index: Similarity and dissimilarity in ruptured and unruptured cerebral aneurysm blebs. *J. Neurosurg.* **2012**, *117*, 774–780. [[CrossRef](#)]
52. Lv, N.; Wang, C.; Karmonik, C.; Fang, Y.; Xu, J.; Yu, Y.; Cao, W.; Liu, J.; Huang, Q. Morphological and hemodynamic discriminators for rupture status in posterior communicating artery aneurysms. *PLoS ONE* **2016**, *11*, e0149906. [[CrossRef](#)]
53. Bernardini, A.; Larrabide, I.; Morales, H.G.; Pennati, G.; Petrini, L.; Cito, S.; Frangi, A.F. Influence of different computational approaches for stent deployment on cerebral aneurysm haemodynamics. *Interface Focus* **2011**, *1*, 338–348. [[CrossRef](#)]
54. He, X.; Ku, D.N. Pulsatile flow in the human left coronary artery bifurcation: Average conditions. *J. Biomech. Eng.* **1996**, *118*, 74–82. [[CrossRef](#)]
55. Himburg, H.A.; Grzybowski, D.M.; Hazel, A.L.; LaMack, J.A.; Li, X.M.; Friedman, M.H. Spatial comparison between wall shear stress measures and porcine arterial endothelial permeability. *Am. J. Physiol. Heart Circ. Physiol.* **2004**, *286*, H1916–H1922. [[CrossRef](#)]
56. Jou, L.D.; Lee, D.H.; Morsi, H.; Mawad, M.E. Wall shear stress on ruptured and unruptured intracranial aneurysms at the internal carotid artery. *AJNR Am. J. Neuroradiol.* **2008**, *29*, 1761–1767. [[CrossRef](#)]
57. Meng, H.; Wang, Z.; Kim, M.; Ecker, R.D.; Hopkins, L.N. Saccular aneurysms on straight and curved vessels are subject to different hemodynamics: Implications of intravascular stenting. *AJNR Am. J. Neuroradiol.* **2006**, *27*, 1861–1865.
58. Ohta, M.; Hirabayashi, M.; Wetzel, S.; Lylyk, P.; Wata, H.; Tsutsumi, S.; Rüfenacht, D.A. Impact of stent design on intra-aneurysmal flow. A computer simulation study. *Interv. Neuroradiol.* **2004**, *10*, 85–94. [[CrossRef](#)]
59. Anzai, H.; Falcone, J.L.; Chopard, B.; Hayase, T.; Ohta, M. Optimization of strut placement in flow diverter stents for four different aneurysm configurations. *J. Biomech. Eng.* **2004**, *136*, 061006. [[CrossRef](#)]
60. Malek, A.M.; Alper, S.L.; Izumo, S. Hemodynamic shear stress and its role in atherosclerosis. *JAMA* **1999**, *282*, 2035–2042. [[CrossRef](#)] [[PubMed](#)]
61. Hayashi, K.; Handa, H.; Nagasawa, S.; Okamura, A.; Moritake, K. Stiffness and elastic behavior of human intracranial and extracranial arteries. *J. Biomech.* **1980**, *13*, 175–184. [[CrossRef](#)]

